AGU ADVANCING EARTH AND SPACE SCIENCE

Geophysical Research Letters

RESEARCH LETTER
10.1029/2021GL093729

Mid-Latitude Thermosphere-Ionosphere Na (TINa) Layers Observed With High-Sensitivity Na Doppler Lidar Over Boulder (40.13°N, 105.24°W)

Xinzhao Chu[1], Yingfei Chen[1], Chihoko Y. Cullens[2], Zhibin Yu[3], Zhonghua Xu[4], Shun-Rong Zhang[5], Wentao Huang[6], Jackson Jandreau[1], Thomas J. Immel[2], and Arthur D. Richmond[7]

[1]Cooperative Institute of Research in Environmental Sciences & Department of Aerospace Engineering Sciences, University of Colorado Boulder, Boulder, CO, USA, [2]Space Sciences Laboratory, University of California Berkeley, Berkeley, CA, USA, [3]Institute of Space Science and Applied Technology, Harbin Institute of Technology (Shenzhen), Shenzhen, China, [4]Bradley Department of Electrical and Computer Engineering, Virginia Polytechnic Institute and State University, Blacksburg, VA, USA, [5]Haystack Observatory, Massachusetts Institute of Technology, Westford, MA, USA, [6]MNR Key Laboratory of Polar Science, Polar Research Institute of China, Shanghai, China, [7]High Altitude Observatory, National Center for Atmospheric Research, Boulder, CO, USA

Abstract We report the first lidar observations of regular occurrence of mid-latitude thermosphere-ionosphere Na (TINa) layers over Boulder (40.13°N, 105.24°W), Colorado. Detection of tenuous Na layers (~0.1–1 cm^{-3} from 150 to 130 km) was enabled by high-sensitivity Na Doppler lidar. TINa layers occur regularly in various months and years, descending from ~125 km after dusk and from ~150 km before dawn. The downward-progression phase speeds are ~3 m/s above 120 km and ~1 m/s below 115 km, consistent with semidiurnal tidal phase speeds. One or more layers sometimes occur across local midnight. Elevated volume mixing ratios above the turning point (~105–110 km) of Na density slope suggest in situ production of the dawn/dusk layers via neutralization of converged Na^+ layers. Vertical drift velocity of $TINa^+$ calculated with the Ionospheric Connection Explorer Hough Mode Extension tidal winds shows convergent ion flow phases aligned well with TINa, supporting this formation hypothesis.

Plain Language Summary Thermosphere-ionosphere metal (TIMt) layers are an intriguing phenomenon discovered 10 years ago in Antarctica. They provide a natural laboratory and tracer to study the complex space-atmosphere interactions in the Earth's thermosphere and ionosphere. TIMt layers have been observed in the neutral Fe (iron), Na (sodium), and K (potassium) species in both the polar and tropical regions but quite rarely at midlatitudes. To date, all reported TIMt layers have an irregular occurrence. This article reports an exciting new discovery made at a mid-latitude site. That is, the TIMt layers in the Na species (thermosphere-ionosphere Na layers) occur fairly regularly before dawn and after dusk. Such regular occurrence of thermosphere-ionosphere Na (TINa) layers is reported for the first time. Such layers are tenuous and their detection is enabled by a Na Doppler lidar developed at the University of Colorado Boulder, which possesses very high detection sensitivity. Utilizing the thermospheric wind data from a new satellite mission (Ionospheric Connection Explorer), it is found that these neutral metal layers are closely related to the tides-driven metal ion layers. The Boulder TINa layers likely provide a new way to study the ion transport in the E to lower F regions.

Key Points:

- Tenuous thermosphere-ionosphere Na (TINa) layers occur regularly descending from ~150 km before dawn and from ~125 km after dusk with semidiurnal tidal phase speeds
- Enhanced mixing ratios above the Na slope turning points suggest in situ production of TINa via neutralization of converged $TINa^+$ layers
- Vertical drift velocity of $TINa^+$ calculated with inferred tidal winds shows convergent flow phases aligned well with Boulder TINa layers

Supporting Information:

Supporting Information may be found in the online version of this article.

Correspondence to:

X. Chu and Z. Yu,
Xinzhao.Chu@Colorado.edu;
yuzb@hit.edu.cn

Citation:

Chu, X., Chen, Y., Cullens, C. Y., Yu, Z., Xu, Z., Zhang, S.-R., et al. (2021). Mid-latitude thermosphere-ionosphere Na (TINa) layers observed with high-sensitivity Na Doppler lidar over Boulder (40.13°N, 105.24°W). *Geophysical Research Letters*, *48*, e2021GL093729. https://doi.org/10.1029/2021GL093729

Received 5 APR 2021
Accepted 15 MAY 2021

1. Introduction

Thermosphere-ionosphere metal (TIMt) layers occur, above the permanent metal layers, in a large altitude range from ~110 to ~200 km (Chu & Yu, 2017; Chu et al., 2011, 2020; Plane et al., 2015). They usually possess broad layer widths and exhibit either gravity-wave or tidal-wave downward phase progression (e.g., Chu et al., 2011, 2020; Gao et al., 2015). Morphologies of TIMt layers are different from the main layer topside (e.g., Höffner & Friedman, 2005) and also distinctly different from sporadic metal layers (Plane, 2003), including high-altitude sporadic metal layers (e.g., Collins et al., 1996; Gardner et al., 2001; Ma & Yi, 2010). Since the first discovery 10 years ago, TIMt layers have attracted research attention because they open a new window to studying fundamental processes in the E–F regions where measurements of the neutral

atmosphere are scarce but plasma-neutral interactions are crucial (e.g., Chu & Yu, 2017; Chu et al., 2020; Huba et al., 2019, 2020; Plane et al., 2015).

The first report of TIMt layers was given by Chu et al. (2011) in Antarctica via lidar observations of thermosphere-ionosphere Fe (TIFe) layers. Neutral metal Fe layers with gravity-wave downward phase progression and periods (~1.5 h) were observed reaching 155 km in May 2011 at McMurdo (77.84°S, 166.67°E). Following this discovery, not only were more TIFe layers observed, but also were other metal species reported, including thermosphere-ionosphere Na (TINa) and K (TIK) layers. At high latitudes, many more TIFe layers were further observed at McMurdo with various morphologies, for example, the June 1, 2013, case reached over 170 km with ~2 h wave period and possessed high Fe density of ~500 cm^{-3} at 140 km (Chu et al., 2016), and numerous cases revealed diurnal variations of TIFe layers (Chu et al., 2020; Yu et al., 2020). TIFe layers were also observed at Davis (69°S) with a tidal phase (Lübken et al., 2011). TINa layers were observed at Syowa (69°S) with a gravity wave phase and period of ~2 h (Tsuda et al., 2015). Recently, Chu et al. (2020) reported the simultaneous observations of TIFe and TINa layers at McMurdo, showing unexpected differences between distinct TIFe and diffuse TINa. At low latitudes, a TIK layer was first reported at Arecibo (18.35°N, 66.75°W) by Friedman et al. (2013), and then TINa layers were reported for Lijiang (26.7°N, 100.0°E) by Gao et al. (2015) and Cerro Pachon (30.25°S, 70.74°W) (Liu et al., 2016; Smith & Chu, 2015), all exhibiting downward tidal-phase progression. The Arecibo TIK layer occurred near sunrise, while both Lijiang and Cerro Pachon showed a single TINa layer across the local midnight. Raizada et al. (2015) reported a simultaneous observation of TINa and TIK at Arecibo, revealing much slower downward phase speed and different occurrence local time than the TIK reported by Friedman et al. (2013). Interestingly, the TINa and TIK layers behaved similarly in the report of Raizada et al. (2015), in contrast to the stunning differences between TINa and TIFe observed at McMurdo (Chu et al., 2020). At midlatitudes (~35°–60°), the occurrence of TIMt layers appeared to be much rarer than at high and low latitudes, and reports to date came from two stations (Yanqing and Pingquan) close to Beijing (40.5°N). Wang et al. (2012) and Xia et al. (2020) reported TINa layers going up to 125 km with clear downward phase progression. Xun et al. (2019) reported four cases of TINa out of 137 nights of lidar observations, with one reaching 196 km. These cases near Beijing do not reveal a consistent trend in the occurrence time, progression phase, or period (Wang et al., 2012; Xia et al., 2020; Xun et al., 2019).

Using a TIFe model, Chu and Yu (2017) replicated the McMurdo observations on May 28, 2011, using a hypothesis that the TIFe layers are produced through neutralization of converged Fe^+ layers via recombination with electrons, where Fe^+ ions are transported and converged by polar electric fields and gravity-wave-induced neutral winds. Chu and Yu (2017) further suggested extrapolating the TIFe theory to help infer a global picture of multiple metal species (e.g., Fe, Mg, Na, K, etc.). For instance, outside the polar regions, the plasma fountain effect at low latitudes due to the equatorial electric fields substitutes for the polar electric fields in transporting metal ions vertically, and gravity-wave-induced wind shears in the polar region are replaced by tidal-wave-driven wind shears. While the polar electric fields and equatorial dynamo electric fields are effective in vertical transport of metal ions at high and low latitudes, the $\vec{E} \times \vec{B}$ drift does not diminish to zero and tidal winds are strong at mid-latitudes. Therefore, in principle TIMt layers should form for mid-latitude sites with recurrent occurrence. However, observing such tenuous TIMt layers is very challenging as it demands high detection sensitivity of lidars. Here, we report the first observations of mid-latitude TINa over Boulder, Colorado, with regular occurrence around dawn and dusk. Possible formation mechanisms are discussed after the observation report.

2. Observations With High-Sensitivity Lidar Over Boulder

TINa observations were made at Table Mountain Observatory (40.13°N, 105.24°W), north Boulder with an advanced resonance-fluorescence lidar, the Student Training and Atmospheric Research (STAR) Na Doppler lidar. This lidar employed a narrowband laser transmitter tuned to the D_{2a} line at 589 nm, and a 3-frequency Doppler-ratio technique to measure Na density, temperature, and vertical wind simultaneously (Chu & Papen, 2005). It was initially constructed with a 40-cm diameter true-Cassegrain telescope in summer 2010, and its data at the levels of ~20–50 counts per laser shot was used in the studies of mesospheric Na and Fe layers (Huang et al., 2013) and their fluxes (Huang et al., 2015). In summer 2011, the lidar was upgraded to an 81-cm diameter prime-focus Newtonian telescope with high-efficiency receiver architecture

(Smith & Chu, 2015). Combined with further updates in laser transmitter later on, the Na signal levels were improved by 20–50 times to ∼1,000–2,000 counts per laser shot, enabling high-sensitivity detection. Such high-quality measurements of vertical winds and temperatures in the mesopause region were used in studies of high-to-medium frequency gravity waves (Lu et al., 2015, 2017).

TINa layers were observed in the nighttime E region (100–150 km) in various months and years. For this first report, we illustrate in Figure 1 the Na number densities, relative density perturbations, and volume mixing ratios for selected nights in November and January when the Na column abundances are high and lidar observations span long nights. The relative Na density perturbations are computed by subtracting the nightly mean profile and then dividing by this mean profile. The Na volume mixing ratios are calculated by dividing the Na density profiles with the corresponding total atmospheric number density profiles at Boulder provided by the MSISE00 model (Picone et al., 2002). Note that 7 UT corresponds to Boulder local midnight, and 1 and 13 UT correspond to dusk and dawn (6 p.m. and 6 a.m. local time). The most distinct feature is a TINa layer broad in time and altitude before dawn, which exhibits ascending features in the envelope of Na total density (e.g., Figure 1a) from 8–9 to ∼12 UT but descending features in the maximum mixing ratio (e.g., Figure 1f) from ∼140 to 150 km around 10–11 UT to ∼120–110 km around 12–13 UT. Such a TINa layer occurs on every night shown here as long as the observations are long enough to cover the sunrise time. Another distinct feature is a concentrated descending TINa layer occurring at dusk, which starts to descend at 1 UT from ∼125–120 to ∼110 km merging with the main metal layers around 4 UT. Between the dusk and dawn layers, a third layer near the local midnight occurs on some nights (e.g., November 11, 2013), but does not show up on the others (e.g., November 2, 2013). Occasionally, more than three layers occur within a night (e.g., January 11, 2014). The classification of dawn, dusk, midnight, and multiple TINa layers based on the limited nights shown in Figure 1 is consistent with a larger database consisting of 7 years (2011–2017) of measurements. The statistical characterization of the TINa layers spanning 7 years is beyond the scope of this work but will be addressed in future work.

To further quantify the TINa observed, the Na density profiles and the volume mixing ratio profiles are plotted in log-10 scales in Figure 2 for the dusk and dawn layers. The time spans of the mean profiles are marked in the figure legends. The log-scale density profiles of dawn layers show a turning point around 110 km, above and below which the slopes are different. Correspondingly, the TINa volume mixing ratio exhibits a weak, broad peak above ∼110 km, very similar to the findings at McMurdo (Chu et al., 2020). The dusk layers exhibit a narrower mixing ratio peak above its density slope turning point that is usually several kilometers lower than that of the dawn layers (except January 23, 2015). Such increased mixing ratios provide strong evidence for *in-situ* production of Na above the turning point (∼105–110 km) for both the dusk and dawn layers as discussed in Chu et al. (2020). Interestingly, the mixing ratio of the dawn layer on January 11, 2014 above the turning point is higher ($\sim 1.3 \times 10^{-11}$) than other nights, and its shape is nearly flat. The dusk layers usually have lower maximum altitudes (∼120–125 km) than those of the dawn layers (∼140–150 km), but the dusk layers on January 23 and 27, 2015, reach over 130 km.

The number densities of TINa occurring above 120 km in Figure 2 are very low. Typical Na densities are 0.1–0.5 cm^{-3} from 150 to 140 km, ∼1 cm^{-3} at 130 km, and 3–5 cm^{-3} at 120 km, which are in general smaller than those at McMurdo (Chu et al., 2020). Fortunately, the STAR lidar had high detection sensitivity (better than 0.1 cm^{-3}) on many nights as shown in Figure 2, enabling the detection of such tenuous TINa layers. The dusk TINa layer has densities and mixing ratios even smaller than the dawn layer. The vertical phase speed roughly estimated by tracking the maximum mixing ratio in Figure 1 is ∼10 km/h, translating to ∼2.7 m/s, which is a typical semidiurnal tidal phase speed from 150 to 130 km (Friedman et al., 2013). The dusk layer is narrower in time span and has a slower vertical phase speed of ∼5 km/h, that is, 1.3 m/s, which is consistent with an average of semidiurnal tidal phase speed from 120 to 105 km (Friedman et al., 2013). Boulder TINa layers have starkly different shapes and phases from those at McMurdo where gravity wave periods with much larger phase speeds are observed (Chu et al., 2020).

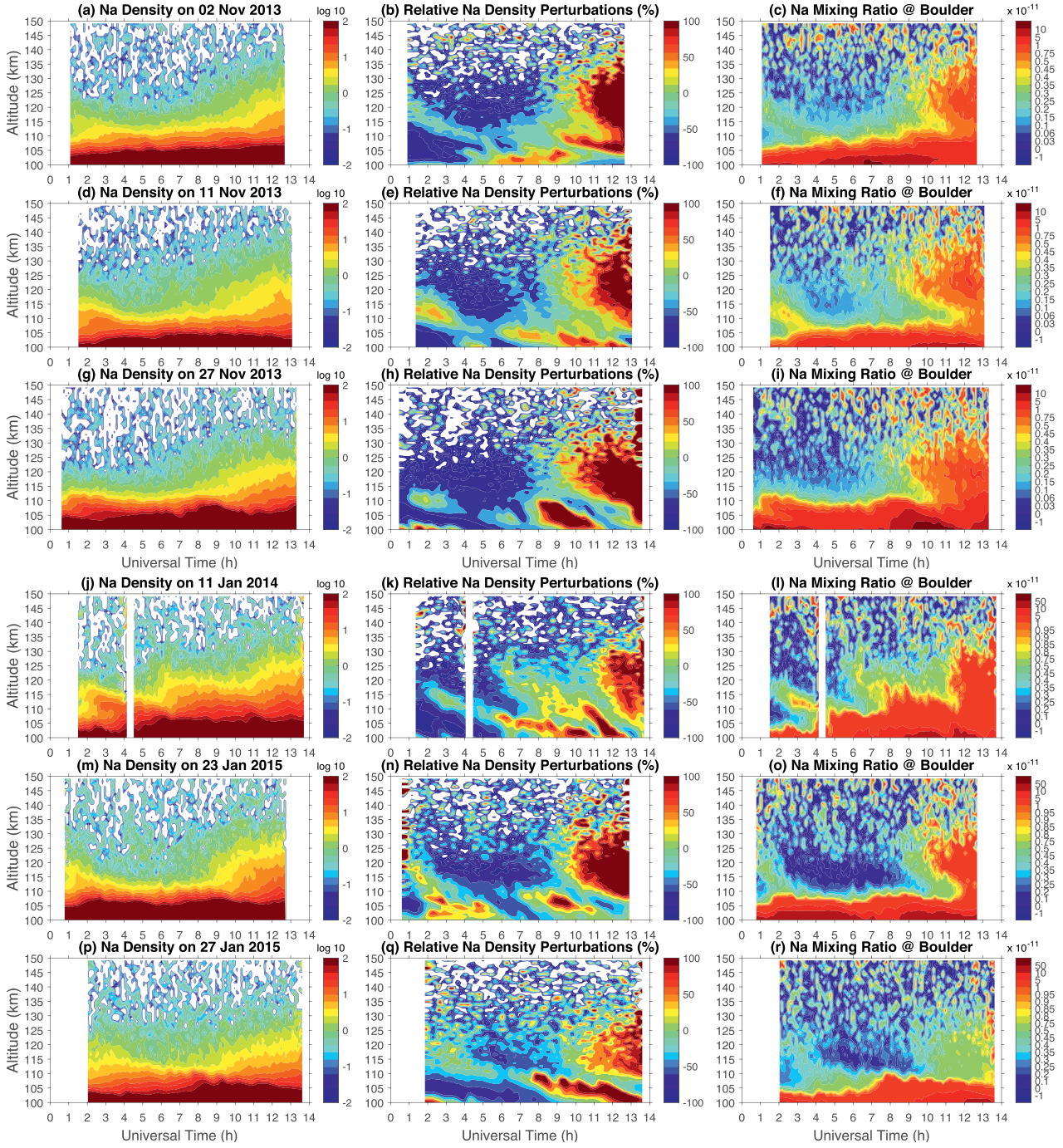

Figure 1. Na Doppler lidar observations of thermosphere-ionosphere Na layers at Boulder over multiple nights. (left) Na number density in log-10 scale. (middle) relative Na density perturbation in percentage. (right) Na volume mixing ratio plotted in uneven color scales. The Na density is retrieved with resolutions of 7.5 min and 960 m. The full range (75–150 km) plots are provided in Supporting Information. Note that 7 UT corresponds to Boulder local midnight.

3. Discussion

Boulder TIMt layers occur at least twice during a night at regular phases (dawn and dusk), in stark contrast to the McMurdo TIMt layers exhibiting gravity-wave phases and periods (Chu et al., 2011, 2020). The low-latitude TIMt layers show tidal phases but a single layer during nighttime observations (Friedman et al., 2013; Gao et al., 2015; Raizada et al., 2015; Smith & Chu, 2015). Interestingly, Boulder dawn layers

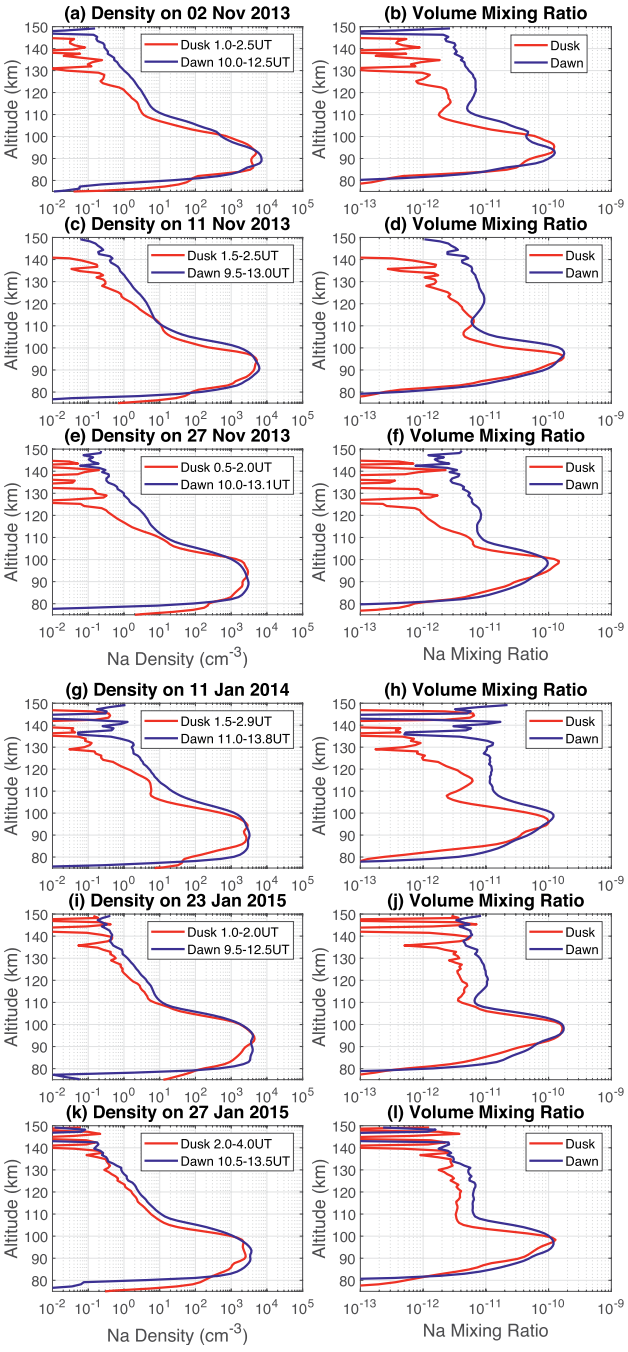

Figure 2. Vertical profiles of Na density and volume mixing ratio for dusk (red) and dawn (blue) layers at Boulder for six nights shown in Figure 1. The Na detection limit is better than 0.1 cm^{-3}. The uncertainty (precision) of Na density varies from ~0.1% at the mesospheric peak to ~2%–10% in the thermosphere-ionosphere Na.

have more complicated motions than the dusk layers. The regularity of TINa layer occurrence and broad peak of mixing ratio above 110 km lead to the hypothesis that the dawn and dusk TINa layers are formed by in situ Na production that is modulated by tidal winds, rather than pure transport of neutral Na.

Pure neutral transport cannot explain the observations because pure vertical transport of neutrals cannot substantially increase its mixing ratio as discussed in Cox et al. (1993) and Chu et al. (2020). The mixing ratios at the turning point around 110 km are smaller than the mixing ratios of the dusk layer around 120 km and dawn layer at 125 km (e.g., November 2 and 11, 2013, cases); therefore, upward diffusion of neutral metals from the main layer below 110 km cannot explain the observed TINa layers with enhanced mixing ratios. Furthermore, the mixing ratios at the top of E region (~150 km) are smaller than the peak mixing ratios of dusk and dawn layers; therefore, downward transport of neutral metals from the top of E region also cannot explain the observations. The mixing ratio results rule out the mechanism of pure neutral transport. Therefore, there must be in situ production of neutral metals along the TIMt layer altitudes.

Two possible mechanisms for neutral Na production include the neutralization of Na^+ ions with electrons and the sputtering of metals off meteoroids. One may argue for the sputtering of metals from meteoroids by air molecules when meteoroids enter the atmosphere. However, there is no reason for sputtering to be correlated with regular tidal phases. First-principle modeling studies show negligible injection rate of metals above 120 km by sputtering (Carrillo-Sanchez et al., 2015, 2016). For rare or sporadic cases like the ones observed at Beijing (Xun et al., 2019) and the simultaneous observations of TINa and TIK at Arecibo (Raizada et al., 2015), we do not rule out the possibility that a strong meteor event deposited a large amount of metals in the atmosphere, and they are horizontally transported over the lidar sites while descending down. Such meteor events would be irregular in local time so could not explain the regular occurrence of TIMt layers at Boulder.

It is necessary to invoke the ion transport and neutralization as modeled in Chu and Yu (2017). From previous modeling, we have learned that both the electric fields and neutral winds can transport ions upward and downward as well as converge ions to form dense ion layers (Bishop & Earle, 2003; Chu & Yu, 2017; Huba et al., 2019). While the polar electric fields are large and provide the major driving force to transport metal ions at McMurdo, the electric fields at midlatitudes (e.g., Buonsanto et al., 1993) are much smaller (several vs. 10s mV/m) than at McMurdo while the tidal horizontal winds are strong at midlatitudes. The regular occurrence of TINa layers with apparent downward phase progression strongly suggests tidal winds playing important roles in the layer formation. Although vertical shears of the horizontal winds cannot converge neutrals, they can converge ions strongly via geomagnetic Lorentz forcing and ion-neutral collisional coupling in the E and lower F regions, as explained in wind shear mechanisms (e.g., Axford, 1963; Haldoupis et al., 2004; Whitehead, 1961, 1989). The vertical drift velocity of Na^+ ions, V_{izw}, induced by neutral winds is given below (Chu & Yu, 2017)

$$V_{izw} = \frac{\xi \cos\theta_D}{1+\xi^2} V_{n,x} - \frac{\sin(2\theta_D)}{2(1+\xi^2)} V_{n,y} + \left(1 - \frac{\cos^2\theta_D}{1+\xi^2}\right) V_{n,z} \quad (1)$$

where ξ is the ratio of ion-neutral collision frequency to the gyro frequency of Na^+ (Figure 3a), θ_D is the dip angle, and V_n is the neutral winds in geomagnetic zonal (x), meridional (y), and vertical (z) coordinates. Because $\theta_D = 66.55°$ for Boulder, the zonal wind factor f_U is positive while the meridional wind factor f_V is negative (see Figure 3b).

$$f_U = \frac{\xi \cos\theta_D}{1+\xi^2} \text{ and } f_V = -\frac{\sin(2\theta_D)}{2(1+\xi^2)} \quad (2)$$

Consequently, eastward and southward (westward and northward) winds transport ions upward (downward). It is clear that zonal wind factor dominates below ~122 km while the meridional wind factor dominates at higher altitudes, and the ion drifts are the combined effects. As the declination angle of the geomagnetic field is only ~8.5° at Boulder, the geographic zonal and meridional directions are close to those of the geomagnetic coordinates. Therefore, the geographic zonal and meridional winds derived from the Ionospheric Connection Explorer (ICON) mission (Immel et al., 2018) are used in the V_{izw} calculation. The Michelson Interferometer for Global High-Resolution Thermospheric Imaging (MIGHTI) instrument on ICON observes temperatures and winds from 90 to 300 km during daytime and from 90 to ~109 km in the night in the latitude range of 10°S–42°N (Englert et al., 2017; Stevens et al., 2018). The tidal neutral winds are obtained by fitting Hough Mode Extensions (HMEs) to MIGHTI wind data. Detailed HME methodologies are summarized in Forbes et al. (1994) and HME for ICON is summarized in Forbes et al. (2017) and Cullens et al. (2020). Although the ICON wind data are in a different year (2020) than the lidar data, the repeated occurrence of dawn/dusk TINa layers in different months and years strongly suggests fairly regular recurring mechanisms like tidal winds. Therefore, to first order it is reasonable to use the ICON wind data to represent the climatological features of thermospheric winds over Boulder. An example of the zonal (U) and meridional (V) tidal winds, averaged over January 1–15, 2020, are shown in Figures 3c and 3d, and the V_{izw} calculated for Na^+ using Equation 1 is shown in Figure 3e.

When considering vertical transport only, the ion density (N_i) time rate of change is $\frac{\partial N_i}{\partial t} \sim -\left(N_i \frac{\partial V_{iz}}{\partial z} + V_{iz} \frac{\partial N_i}{\partial z}\right)$, where V_{iz} is the total vertical drift velocity of ions. Consequently, descending convergent ion layers are expected where dV_{iz}/dz is negative and V_{iz} approximately equals the phase velocity of descending contours, as around 1 UT at ~115 km and around 11 UT at ~145 km in Figure 3e. This is the situation illustrated at the left of Figure 3f. The Na produced by Na^+ neutralization in such a descending layer will tend to accumulate above the $TINa^+$ layer so that a TINa layer peak may lie above the $TINa^+$ layer peak. For a convergent region of ascending $TINa^+$ like that at 7 UT around 135 km (illustrated by the second sketch in Figure 3f), the TINa density peak may lie below the $TINa^+$ peak. Modeling will be necessary to fully understand the spatial and temporal relations between $TINa^+$ and TINa layers. Nonetheless, there is a close relation between features of V_{izw} in Figure 3e and relative Na density perturbations in Figure 1. From 0 to 4 UT, the ion convergence phase is limited to a narrow altitude range (from ~120 to ~105 km) with downward phase progression following the downward ion flow. The phase speed is ~1.3 m/s, agreeing with the well-confined TINa layers observed after dusk on November 2 and 11, 2013. Passing local midnight (7 UT), the tidal winds start to transport Na^+ upward above 112 km, and the maximum upward drift is ~5 m/s around 9 UT and 124 km. The faster drifting ions can catch up with the slower drifting ions around 130–140 km, accumulating Na^+ ions at ~9 UT. Such convergent flow occurs in a wide altitude and time range because of the ion-drift velocity gradient; therefore, Na^+ ion accumulation could span over several hours from ~8 to 9 UT to the end of nighttime lidar observations, and also in a relatively large altitude range from 150 to ~115 km. Such ion convergent range and time are consistent with the broad TINa distributions observed, and the phase speed of ~3 m/s is also consistent with the TINa downward phase speed before dawn.

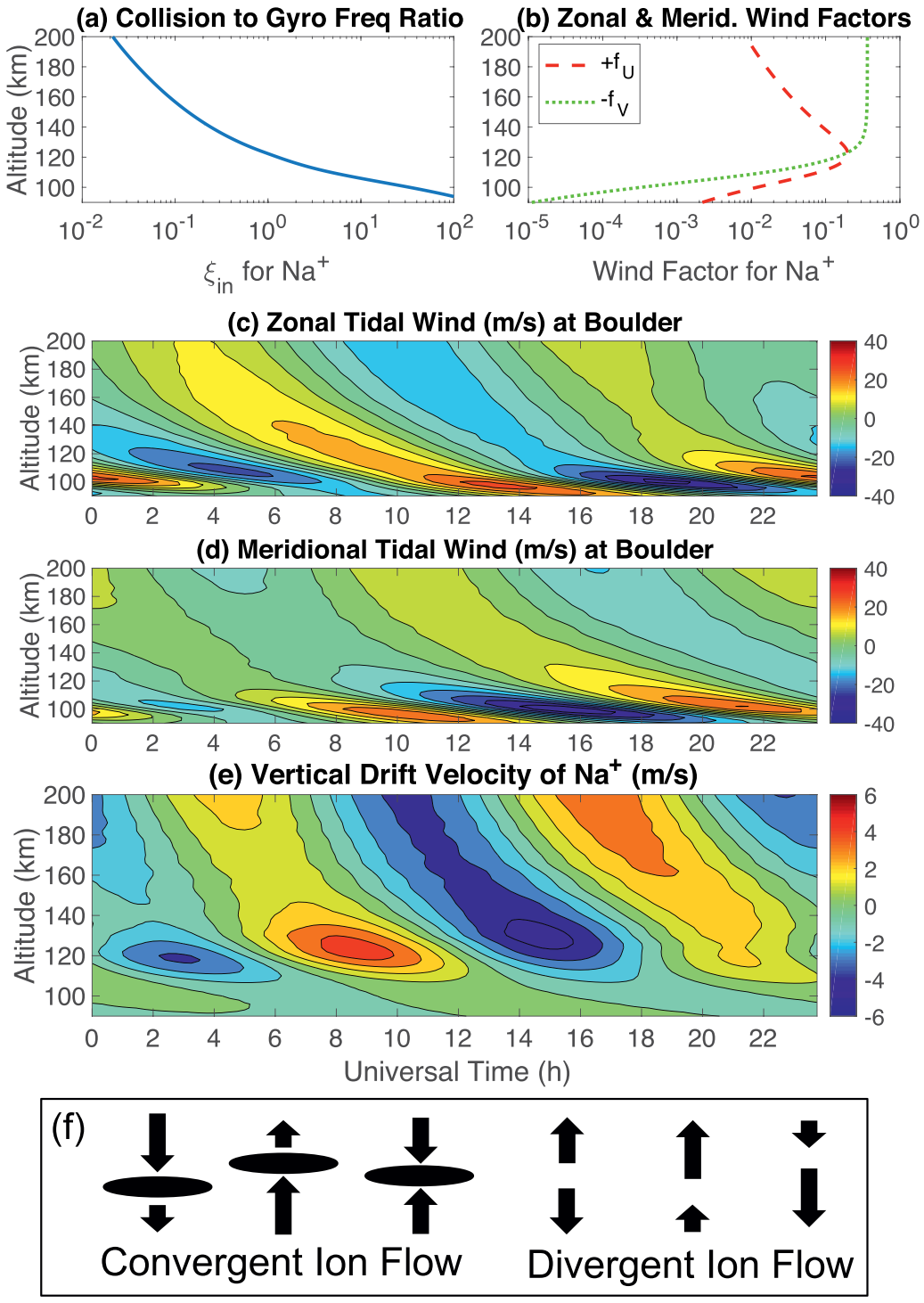

Figure 3. (a) The ratio of Na^+ ion-neutral collision frequency to gyro frequency, (b) the zonal and meridional wind factors for Na^+. (c) Zonal and (d) meridional tidal winds constructed from Hough Mode Extension from ICON mission (positive is eastward and northward, respectively). (e) Vertical drift velocity of Na^+ ions for Boulder (positive is upward). (f) Sketch of convergent and divergent flows of ions, inspired by Chu and Yu (2017).

Buonsanto et al. (1993) reported the statistical mean of F-region ion transport at Millstone Hill (42.6°N, 72.6°W) using an incoherent scatter radar (ISR), where geographic and geomagnetic latitudes are similar to Boulder. The diurnal variation of $V_{\perp N}$ (northward ion drift velocity perpendicular to the magnetic field line) shows a reversal from northward to southward drifts near noon, and a return to northward drifts in the pre-midnight hours, see Figure 1 winter panel in Buonsanto et al. (1993). The ISR-measured F-region ion drifts perpendicular to $\vec{B}$ in the meridional plane represent the electric field effects. Assuming the mid-latitude E region has similar electric field effects, the pre-midnight return to northward (thereby upward) perpendicular drifts is in phase with the tidal-wind-induced upward ion transport before dawn, and the electric-field-induced southward drifts after noon are also consistent with the tidal-wind-induced downward ion transport at dusk. The combination of the tidal wind and electric field effects on ion transport likely produces the converged Na^+ layers near dusk and dawn phases. These ion layers undergo neutralization processes via direct and dissociative recombination with electrons (Plane, 2003; Plane et al., 2015) and convert a tiny portion of metal ions to neutrals. As modeled in Chu and Yu (2017) for TIFe, less than 1% neutralization of converged ions is sufficient to produce the neutral metals observed. Such hypothesis provides the most likely explanation to the regular occurrence of TINa layers in the E region over Boulder. The real situations could be more complicated because of a time lag between ion convergence and N_i, and the $\frac{\partial N_i}{\partial t}$ dependence on $\frac{\partial V_{iz}}{\partial z}$ and V_{iz} when $\frac{\partial N_i}{\partial z} \neq 0$. Also, the altitudes of peak TINa and $TINa^+$ densities do not necessarily coincide because of a time lag associated with recombination and possible height variations of Na diffusion and loss (Yu, 2014). Future simulations are necessary to study the relation of TINa with $TINa^+$ convergent flow, expanding from the TIFe modeling work.

4. Conclusions

The STAR Na Doppler lidar with high detection sensitivities has enabled the discovery of mid-latitude TINa layers in the E region with fairly regular occurrence over Boulder. A TINa layer descends from ~125 km after dusk and merges with the main layer around 4 UT. Another TINa layer occurs broad in time and altitude before dawn with an ascending envelope of Na total density but a descending maximum mixing ratio starting from ~150 km. The downward-progression phase speeds are ~3 m/s above 120 km and ~1 m/s below 115 km, consistent with semidiurnal tidal phase speeds over Boulder as derived from HME tidal winds of the ICON mission. Occasionally, one or several layers occur across local midnight or between the dusk and dawn layers. Typical number densities of the dawn TINa layers are ~0.1–0.5 cm^{-3} from 150 to 140 km, ~1 cm^{-3} at 130 km, and 3–5 cm^{-3} at 120 km. The Boulder TINa layers exhibit a similar turning point around 110 km as McMurdo, above and below which both the log-scale density and mixing-ratio profiles change to different slopes or trends. The broad peak of mixing ratios above the turning point in Figure 2 rules out pure neutral Na transport from below or from above but provides strong evidence for in situ production of the dawn/dusk neutral TINa layers.

The most probable formation mechanism of TINa is the neutralization of tidal Na^+ layers via recombination with electrons, where $TINa^+$ ions are transported and converged by tidal winds and electric fields. The vertical drift velocity of $TINa^+$ calculated using ICON-HME tidal winds shows convergent flow phases agreeing with the phases (time and altitude) of observed dusk and dawn TINa layers, likely explaining the recurrent occurrence of these dusk and dawn TIMt layers at semidiurnal tidal phases with enhanced mixing ratios. Numerical simulations and multiple-instrument measurements of neutral and ionized metals as well as electron densities are needed to verify the hypothesis and investigate detailed formation mechanisms. Boulder TINa dawn layers occur all year round, including summer months, but the dusk layers occur less frequently. As for the irregular layers occurring between dusk and dawn, some midnight layers even reach ~170 km. Full characterization of Boulder TINa layers and their formation mechanisms are beyond the scope of this paper but will be addressed in future studies.

The TINa detection is unequivocal but such low density demands very high detection sensitivities (better than 0.1 cm^{-3}). Most Na lidars operated in the world had/have the detection limits above a few cm^{-3} and signal levels well below that achieved by the STAR lidar (Smith & Chu, 2015), so the TINa signals would be buried in their background noise. Indeed, an earlier version of the STAR lidar, before it was upgraded

to high-sensitivity, was not able to detect TINa layers above 115 km (Huang et al., 2013). Therefore, it is understandable why many years of lidar observations at midlatitudes did not discover such TINa layers until this report. In the future, lidars with high detection sensitivity enabled by large-aperture telescope, high-efficiency receiver architecture, and powerful transmitter will likely lead to the detection of tenuous TIMt layers globally. These layers provide a natural laboratory for studying the ion-neutral coupling and act as tracers for profiling the neutral wind and temperature in the E to lower F regions. Observing these metal layers also provides a unique way of monitoring vertical transport in the thermosphere and ionosphere.

Data Availability Statement

The data shown in this work can be downloaded online (from https://data.mendeley.com/datasets/nshhxnmrzh/2).

Acknowledgments
The authors sincerely appreciate Weichun Fong and John A. Smith for their significant contributions to the STAR lidar development and receiver improvements. The authors are grateful to Jeffery Forbes for invaluable discussions on tidal winds. The authors offer special thanks to Scott P. Sandberg and Mike Hardesty for their tremendous help in setting up the Table Mountain Lidar Observatory. This work was supported by the National Science Foundation grants AGS-1452351, AGS-2029162, and OPP-1443726. The work of ZHX was supported by NSF grant OPP-1744828. SRZ acknowledges support from AFOSR MURI grant FA9559-16-1-0364 and NSF award AGS-2033787.

References

Axford, W. I. (1963). The formation and vertical movement of dense ionized layers in the ionosphere due to neutral wind shears. *Journal of Geophysical Research*, *68*(3), 769–779. https://doi.org/10.1029/JZ068i003p00769

Bishop, R. L., & Earle, G. D. (2003). Metallic ion transport associated with midlatitude intermediate layer development. *Journal of Geophysical Research*, *108*, 1019. https://doi.org/10.1029/2002JA009411

Buonsanto, M. J., Hagan, M. E., Salah, J. E., & Fejer, B. G. (1993). Solar cycle and seasonal variations inFregion electrodynamics at Millstone Hill. *Journal of Geophysical Research*, *98*, 15677–15683. https://doi.org/10.1029/93ja01187

Carrillo-Sánchez, J. D., Nesvorný, D., Pokorný, P., Janches, D., & Plane, J. M. C. (2016). Sources of cosmic dust in the Earth's atmosphere. *Geophysical Research Letters*, *43*, 11979–11986. https://doi.org/10.1002/2016GL071697

Carrillo-Sánchez, J. D., Plane, J. M. C., Feng, W., Nesvorný, D., & Janches, D. (2015). On the size and velocity distribution of cosmic dust particles entering the atmosphere. *Geophysical Research Letters*, *42*, 6518–6525. https://doi.org/10.1002/2015GL065149

Chu, X., Nishimura, Y., Xu, Z., Yu, Z., Plane, J. M. C., Gardner, C. S., & Ogawa, Y. (2020). First simultaneous lidar observations of thermosphere-ionosphere Fe and Na (TIFe and TINa) layers at McMurdo (77.84°S, 166.67°E), Antarctica with concurrent measurements of aurora activity, enhanced ionization layers, and converging electric field. *Geophysical Research Letters*, *47*. https://doi.org/10.1029/2020GL090181

Chu, X., & Papen, G. (2005). Resonance fluorescence lidar for measurements of the middle and upper atmosphere. In T. Fujii, & T. Fukuchi (Eds.), *Laser remote sensing* (pp. 179–432). Boca Raton, FL: CRC Press. https://doi.org/10.1201/9781420030754

Chu, X., & Yu, Z. (2017). Formation mechanisms of neutral Fe layers in the thermosphere at Antarctica studied with a thermosphere-ionosphere Fe/Fe^+ (TIFe) model. *Journal of Geophysical Research: Space Physics*, *122*, 6812–6848. https://doi.org/10.1002/2016JA023773

Chu, X., Yu, Z., Fong, W., Chen, C., Zhao, J., Barry, I. F., et al. (2016). From Antarctica lidar discoveries to OASIS exploration. EPJ Web of conferences invited paper in Proceedings of the 27th international laser radar conference, New York, July 2015. (Vol. 119, p. 12001). https://doi.org/10.1051/epjconf/201611912001

Chu, X., Yu, Z., Gardner, C. S., Chen, C., & Fong, W. (2011). Lidar observations of neutral Fe layers and fast gravity waves in the thermosphere (110–155 km) at McMurdo (77.8°S, 166.7°E), Antarctica. *Geophysical Research Letters*, *38*(23). https://doi.org/10.1029/2011GL050016

Collins, R. L., Hallinan, T. J., Smith, R. W., & Hernandez, G. (1996). Lidar observations of a large high-altitude sporadic Na layer during active aurora. *Geophysical Research Letters*, *23*(24), 3655–3658. https://doi.org/10.1029/96GL03337

Cox, R. M., Plane, J. M. C., & Green, J. S. A. (1993). A modeling investigation of sudden sodium layers. *Geophysical Research Letters*, *20*, 2841–2844. https://doi.org/10.1029/93GL03002

Cullens, C. Y., Immel, T. J., Triplett, C. C., Wu, Y.-J., England, S. L., Forbes, J. M., & Liu, G. (2020). Sensitivity study for ICON tidal analysis. *Progress in Earth and Planetary Science*, *7*, 18. https://doi.org/10.1186/s40645-020-00330-6

Englert, C. R., Harlander, J. M., Brown, C. M., Marr, K. D., Miller, I. J., Stump, J. E., et al. (2017). Michelson interferometer for global high-resolution thermospheric imaging (MIGHTI): Instrument design and calibration. *Space Science Reviews*, *212*, 553–584. https://doi.org/10.1007/s11214-017-0358-4

Forbes, J. M., Manson, A. H., Vincent, R. A., Fraser, G. J., Vial, F., Wand, R., et al. (1994). Semidiurnal tide in the 80–150 km region: An assimilative data analysis. *Journal of Atmospheric and Terrestrial Physics*, *56*, 1237–1249. https://doi.org/10.1016/0021-9169(94)90062-0

Forbes, J. M., Zhang, X., Hagan, M. E., England, S. L., Liu, G., & Gasperini, F. (2017). On the specification of upward-propagating tides for ICON science investigations. *Space Science Reviews*, *212*, 697–713. https://doi.org/10.1007/s11214-017-0401-5

Friedman, J. S., Chu, X., Brum, C. G. M., & Lu, X. (2013). Observation of a thermospheric descending layer of neutral K over Arecibo. *Journal of Atmospheric and Solar-Terrestrial Physics*, *104*, 253–259. https://doi.org/10.1016/j.jastp.2013.03.002

Gao, Q., Chu, X., Xue, X., Dou, X., Chen, T., & Chen, J. (2015). Lidar observations of thermospheric Na layers up to 170 km with a descending tidal phase at Lijiang (26.7°N, 100.0°E), China. *Journal of Geophysical Research: Space Physics*, *120*, 9213–9220. https://doi.org/10.1002/2015JA021808

Gardner, C. S., Papen, G. C., Chu, X., & Pan, W. (2001). First lidar observations of middle atmosphere temperatures, Fe densities, and polar mesospheric clouds over the North and South Poles. *Geophysical Research Letters*, *28*, 1199–1202. https://doi.org/10.1029/2000GL012622

Haldoupis, C., Pancheva, D., & Mitchell, N. J. (2004). A study of tidal and planetary wave periodicities present in midlatitude sporadicE-layers. *Journal of Geophysical Research*, *109*. https://doi.org/10.1029/2003JA010253

Höffner, J., & Friedman, J. S. (2005). The mesospheric metal layer topside: Examples of simultaneous metal observations. *Journal of Atmospheric and Solar-Terrestrial Physics*, *67*, 1226–1237. https://doi.org/10.1016/J.JASTP.2005.06.010

Huang, W., Chu, X., Gardner, C. S., Carrillo-Sánchez, J. D., Feng, W., Plane, J. M. C., & Nesvorný, D. (2015). Measurements of the vertical fluxes of atomic Fe and Na at the mesopause: Implications for the velocity of cosmic dust entering the atmosphere. *Geophysical Research Letters*, *42*(1), 169–175. https://doi.org/10.1002/2014GL062390

Huang, W., Chu, X., Gardner, C. S., Wang, Z., Fong, W., Smith, J. A., & Roberts, B. R. (2013). Simultaneous, common-volume lidar observations and theoretical studies of correlations among Fe/Na layers and temperatures in the mesosphere and lower thermosphere at Boulder Table Mountain (40°N, 105°W), Colorado. *Journal of Geophysical Research - D: Atmospheres*, *118*(15), 8748–8759. https://doi.org/10.1002/jgrd.50670

Huba, J. D., Krall, J., & Drob, D. (2019). Global ionospheric metal ion transport with SAMI3. *Geophysical Research Letters*, *46*, 7937–7944. https://doi.org/10.1029/2019GL083583

Huba, J. D., Krall, J., & Drob, D. (2020). Modeling the impact of metallic ion layers on equatorial spread with SAMI3/ESF. *Geophysical Research Letters*, *47*. e2020GL087224. https://doi.org/10.1029/2020GL087224

Immel, T. J., England, S. L., Mende, S. B., Heelis, R. A., Englert, C. R., Edelstein, J., et al. (2018). The Ionospheric Connection Explorer mission: Mission goals and design. *Space Science Reviews*, *214*. https://doi.org/10.1007/s11214-017-0449-2

Liu, A. Z., Guo, Y., Vargas, F., & Swenson, G. R. (2016). First measurement of horizontal wind and temperature in the lower thermosphere (105–140 km) with a Na Lidar at Andes Lidar Observatory. *Geophysical Research Letters*, *43*, 2374–2380. https://doi.org/10.1002/2016GL068461

Lu, X., Chen, C., Huang, W., Smith, J. A., Chu, X., Yuan, T., et al. (2015). A coordinated study of 1 h mesoscale gravity waves propagating from Logan to Boulder with CRRL Na Doppler lidars and temperature mapper. *Journal of Geophysical Research - D: Atmospheres*, *120*(19), 10006–10021. https://doi.org/10.1002/2015JD023604

Lu, X., Chu, X., Li, H., Chen, C., Smith, J. A., & Vadas, S. L. (2017). Statistical characterization of high-to-medium frequency mesoscale gravity waves by lidar-measured vertical winds and temperatures in the MLT. *Journal of Atmospheric and Solar-Terrestrial Physics*, *162*, 3–15. https://doi.org/10.1016/j.jastp.2016.10.009

Lübken, F.-J., Höffner, J., Viehl, T. P., Kaifler, B., & Morris, R. J. (2011). First measurements of thermal tides in the summer mesopause region at Antarctic latitudes. *Geophysical Research Letters*, *38*. L24806. https://doi.org/10.1029/2011GL050045

Ma, Z., & Yi, F. (2010). High-altitude sporadic metal atom layers observed with Na and Fe lidars at 30°N. *Journal of Atmospheric and Solar-Terrestrial Physics*, *72*(5–6), 482–491. https://doi.org/10.1016/j.jastp.2010.01.005

Picone, J. M., Hedin, A. E., Drob, D. P., & Aikin, A. C. (2002). NRLMSISE-00 empirical model of the atmosphere: Statistical comparisons and scientific issues. *Journal of Geophysical Research*, *107*(A12), 15-1–15-16. https://doi.org/10.1029/2002JA009430

Plane, J. M. C. (2003). Atmospheric chemistry of meteoric metals. *Chemical Reviews*, *103*(12), 4963–4984. https://doi.org/10.1021/cr0205309

Plane, J. M. C., Feng, W., & Dawkins, E. C. M. (2015). The mesosphere and metals: Chemistry and changes. *Chemical Reviews*, *115*, 4497–4541. https://doi.org/10.1021/cr500501m

Raizada, S., Brum, C. M., Tepley, C. A., Lautenbach, J., Friedman, J. S., Mathews, J. D., et al. (2015). First simultaneous measurements of Na and K thermospheric layers along with TILs from Arecibo. *Geophysical Research Letters*, *42*, 10106–10112. https://doi.org/10.1002/2015GL066714

Smith, J. A., & Chu, X. (2015). High-efficiency receiver architecture for resonance-fluorescence and doppler lidars. *Applied Optics*, *54*, 3173–3184. https://doi.org/10.1364/AO.54.003173

Stevens, M. H., Englert, C. R., Harlander, J. M., England, S. L., Marr, K. D., Brown, C. M., & Immel, T. J. (2018). Retrieval of lower thermospheric temperatures from O2 A band emission: The MIGHTI experiment on ICON. *Space Science Reviews*, *214*, 4. https://doi.org/10.1007/s11214-017-0434-9

Tsuda, T. T., Chu, X., Nakamura, T., Ejiri, M. K., Kawahara, T. D., Yukimatu, A. S., & Hosokawa, K. (2015). A thermospheric Na layer event observed up to 140 km over Syowa Station (69.0°S, 39.6°E) in Antarctica. *Geophysical Research Letters*, *42*, 3647–3653. https://doi.org/10.1002/2015GL064101

Wang, J., Yang, Y., Cheng, X., Yang, G., Song, S., & Gong, S. (2012). Double sodium layers observation over Beijing, China. *Geophysical Research Letters*, *39*. L15801. https://doi.org/10.1029/2012GL052134

Whitehead, J. D. (1961). The formation of the sporadic-E layer in the temperate zones. *Journal of Atmospheric and Terrestrial Physics*, *20*(1), 49–58. https://doi.org/10.1016/0021-9169(61)90097-6

Whitehead, J. D. (1989). Recent work on mid-latitude and equatorial sporadic-E. *Journal of Atmospheric and Terrestrial Physics*, *51*, 401–424. https://doi.org/10.1016/0021-9169(89)90122-0

Xia, Y., Cheng, X., Li, F., Yang, Y., Jiao, J., Xun, Y., et al. (2020). Diurnal variation of atmospheric metal Na layer and nighttime top extension detected by a Na lidar with narrowband spectral filters at Beijing, China. *Journal of Quantitative Spectroscopy and Radiative Transfer*, *255*, 107256. https://doi.org/10.1016/j.jqsrt.2020.107256

Xun, Y., Yang, G., She, C. Y., Wang, J., Du, L., Yan, Z., et al. (2019). The first concurrent observations of thermospheric Na layers from two nearby central midlatitude lidar stations. *Geophysical Research Letters*, *46*, 1892–1899. https://doi.org/10.1029/2018GL081645

Yu, Z. (2014). *Lidar observations and numerical modeling studies of thermospheric metal layers and solar effects on mesospheric Fe layers*. PhD dissertation, Boulder, CO: University of Colorado Boulder.

Yu, Z., Chu, X., Lu, X, & Chen, C (2020). Dynamic drivers of TIFe diurnal cycle in Antarctica. *EPJ Web of Conferences*, *237*, 04002. https://doi.org/10.1051/epjconf/202023704002